SCIPEDIA Revista Internacional de Métodos Numéricos para Cálculo y Diseño en Ingeniería

Revista Internacional Métodos numéricos para cálculo y diseño en ingeniería RIMNI

In cooperation with CIMNE

Study on the Annular Pressure Prediction Method for Ultra-Deep Well Hydraulic Lift Dual-Gradient Drilling

Yufei Chen[1], Jinping Yuan[1], Kerou Liu[1], Jingyu Zhu[2], Mu Li[1,*], Hao Wang[1] and Yafei Li[1]

[1]CNPC Engineering Technology R&D Company Limited, Beijing, 102206, China

[2]China Petroleum Engineering Co., Ltd. Company, Beijing, 100085, China

ABSTRACT

With the ongoing advancement of oil and gas exploration into deep and ultra-deep formations in China, precise wellbore pressure control under complex geological conditions has become a critical technical challenge for safe drilling operations. To overcome the limitations of existing dual-gradient drilling (DGD) technologies—particularly their poor applicability and limited pressure regulation capability in land-based drilling—this study introduces an innovative hydraulic-lift dual-gradient drilling annular flow model, tailored for ultra-deep vertical wells. The model accounts for solid–liquid phase separation flow characteristics and the hydraulic-lift effect of downhole dual-gradient pumps. The Stability Enhancing Two-Step (SETS) method is employed to solve the strongly nonlinear, coupled governing equations, significantly improving computational stability and efficiency. Experimental validation reveals that the model's predicted pressure distribution closely matches measured data, with a maximum average error of only 16.4%, confirming the model's accuracy and applicability. Additionally, this study systematically analyzes the impact of key parameters—such as drilling fluid flow rate, viscosity, lift pump speed, and the number of pump sections—on bottomhole pressure regulation, providing valuable insights into their influence on annular pressure behavior. The findings offer a solid theoretical foundation for optimizing drilling parameters and ensuring safe, efficient drilling in ultra-deep wells under challenging geological conditions.

OPEN ACCESS

Received: 16/07/2025

Accepted: 19/08/2025

DOI
10.23967/j.rimni.2025.10.70434

Keywords:
Annular pressure
dual-gradient drilling
hydraulic lift
ultra-deep well
pressure control

1 Introduction

Deep oil and gas resources are abundant and hold substantial development potential, with exploration and production activities progressively advancing into deep and ultra-deep formations. In China, deep and ultra-deep oil and gas resources account for approximately 34% of total reserves, with deep oil and natural gas resources comprising 39% and 57%, respectively [1]. Onshore deep and ultra-deep resources are primarily concentrated in the Tarim and Sichuan Basins, where complex geological structures present significant challenges, including high temperature and high pressure,

*Correspondence: Mu Li (limudr@cnpc.com.cn).

multiple pressure systems, and the presence of corrosive acid fluids [2]. Under such harsh conditions, improper handling of wellbore overflow or loss can easily escalate into severe secondary incidents such as pipe sticking, blowouts, and wellbore collapse. Therefore, the development of advanced drilling technologies capable of achieving precise wellbore pressure control is of urgent importance.

Controlled pressure drilling (CPD) technologies mainly include bottomhole constant-pressure drilling and dual-gradient drilling (DGD). The bottomhole constant-pressure drilling technique achieves precise annular pressure control through a combination of backpressure pumps and choke manifold systems [3]. However, its limitation lies in the inability to actively adjust bottomhole pressure, restricting its applicability to addressing overflow incidents alone. By contrast, DGD establishes two distinct pressure gradients within the wellbore through various mechanisms, enabling better adaptation to the narrow pressure window. To date, multiple DGD systems tailored for deepwater applications have been developed worldwide, including subsea mud-lift DGD systems [4], riserless mud recovery (RMR) systems [5], and dual-density mud systems [6]. Nevertheless, these existing systems face persistent issues such as high operational costs, large downhole space requirements, limited density-reduction capability, and poor adaptability to onshore operations. In particular, recent studies on double-layer pipe dual-gradient drilling have explored its feasibility, interface stability, hydraulic modeling, and parameter optimization, providing valuable insights into its application in deepwater and potentially onshore environments [7,8]. Most are designed for marine environments, making direct application to land-based drilling difficult.

To address these limitations, CNPC Engineering Technology R&D Company Limited has developed an innovative DGD approach—Hydraulic-Lift DGD. In this method, a surface pump delivers power fluid to modular circulation connection devices such as top-drive adapters and three-channel drill strings, which then drive a downhole lift pump to achieve dual regulation of flow rate and pressure. While previous modeling efforts for double-layer pipe dual-gradient drilling have addressed aspects such as wellbore pressure calculation and control algorithms [9,10], the theoretical framework for full-wellbore annular pressure prediction for Hydraulic-Lift DGD remains incomplete, necessitating further research to establish a robust basis for parameter optimization and field application. Experimental prototypes have been successfully developed, and laboratory tests have demonstrated effective annular pressure regulation.

Cuttings transport in the annulus has a significant influence on pressure behavior, making it essential to incorporate cuttings migration effects to enhance prediction accuracy. In oil and gas well engineering, solid–liquid two-phase flow models are generally categorized as homogeneous flow models, phase-separated flow models, and drift-flow models. Gavignet and Sobey [11] developed a two-layer steady-state cuttings transport model for inclined and horizontal wells, consisting of a pure fluid layer and a cuttings bed layer. Martins et al. [12], building on the work of Doron et al. [13], proposed a similar two-layer model in which cuttings are transported both through an upper solid–liquid mixed-flow layer and a lower cuttings bed layer, assuming the upper layer behaves as a homogeneous flow. Santan et al. [14] refined this model by distinguishing the velocity differences between solid and liquid phases in the suspension layer, thereby forming a solid–liquid phase separation model with advantages in annular pressure prediction. This approach was later applied to transient cuttings transport modeling [15]. Sun et al. [16] developed a transient cuttings transport model based on the drift-flow concept, treating the solid–liquid mixture as a homogeneous phase without stratification, replacing bed height with cuttings concentration, and using projection algorithms to improve computational efficiency. Related theoretical studies have also explored Newtonian coating flows using two-parameter blade families [17] and non-Newtonian fluid flows over deformable

rotating disks [18], which broaden the understanding of complex fluid dynamics in engineering applications.

Building upon the theory of solid–liquid phase separation, this study develops a transient annular flow model for hydraulic-lift DGD, fully accounting for cuttings migration in vertical wells and the hydraulic-lift effect of downhole dual-gradient pumps. This model enables dynamic prediction of annular pressure profiles throughout the wellbore during DGD operations, thereby elucidating the significant role of Hydraulic-Lift DGD in bottomhole pressure regulation and providing a sound theoretical foundation for parameter optimization and field implementation.

2 Model Building

2.1 Assumptions

In general, for large-displacement wells, cuttings within the wellbore typically exhibit two distinct distribution states: a cuttings bed and a suspended layer [19]. However, in the vertical wellbore section, cuttings rarely settle, making it difficult to form a stable cuttings bed. In such cases, the wellbore is dominated by a suspended layer, with cuttings primarily transported upward by the drilling fluid in a suspended state. Consequently, this study departs from the conventional two-layer cuttings dynamic model commonly applied to large-displacement wells, aiming instead to develop a solid–liquid two-phase mixed-flow model tailored for vertical wellbore sections. The dynamic schematic of the proposed model is presented in Fig. 1, as illustrated by the two-phase flow structure, which clearly depicts the flow behavior and interaction between the solid and liquid phases.

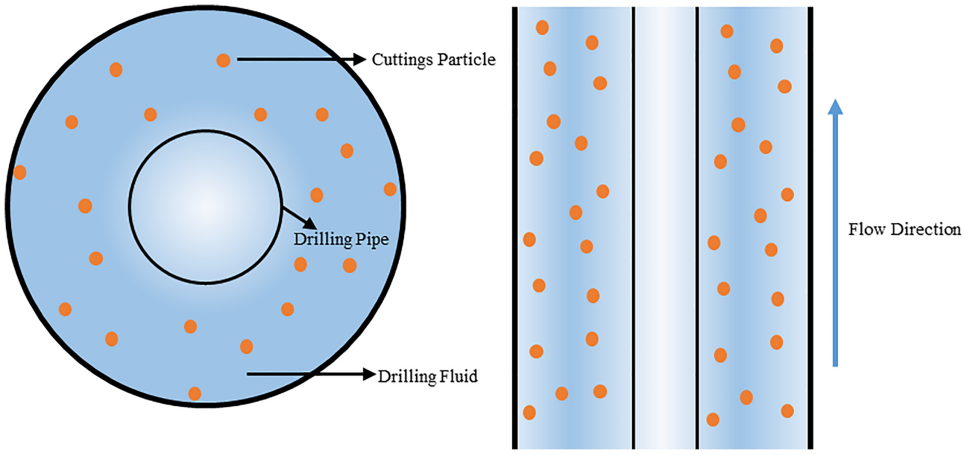

Figure 1: Schematic diagram of mixed-phase flow dynamic model

Given the complexity of computational modeling, the following assumptions are adopted [20,21]:

(1) The solid–liquid phase mixture is treated as an incompressible fluid, with relative slip between the two phases taken into account;

(2) The physical properties of the drilling fluid and cuttings are considered continuous;

(3) The flow of both liquid and solid phases is modeled as one-dimensional along the axial direction;

(4) All cuttings' particles are assumed to be spherical, with uniform diameter and density.

2.2 Solid-Liquid Two-Phase Flow Equation

The continuity equations for each phase are derived from the principle of mass conservation, whereas the momentum equations are formulated based on the principle of momentum conservation. The continuity and momentum equations for the solid–liquid two-phase flow are adapted from the two-layer transient cuttings transport model proposed by Chen et al. (2022) [21]. In the present study, the original equations are modified by removing the cuttings-bed layer, making them applicable to vertical wellbore sections dominated by a suspended layer. The continuity and momentum equations can be expressed as follows:

(a) Liquid phase continuity equation:

$$\frac{\partial}{\partial t}(\varepsilon_l \rho_l) + \frac{\partial}{\partial z}(\varepsilon_l \rho_l u_l) = 0 \tag{1}$$

where ε_l is the volume fraction of the liquid phase, ρ_l is the density of the liquid phase, kg/m^3, u_l is the liquid phase velocity, m/s.

(b) Solid phase continuity equation:

$$\frac{\partial}{\partial t}(\varepsilon_s \rho_s) + \frac{\partial}{\partial z}(\varepsilon_s \rho_s v_s) = 0 \tag{2}$$

where ε_s is the volume fraction of the solid phase, ρ_s is the density of the solid phase, kg/m^3; v_s is the velocity of the solid phase, where the solid phase velocity represents the average velocity vector of the particles, m/s.

(c) Liquid phase momentum equation:

$$\frac{\partial}{\partial t}(\varepsilon_l \rho_l u_l A_h) + \frac{\partial}{\partial z}(\varepsilon_l \rho_l u_l u_l A_h) = -\varepsilon_l A_h \frac{\partial P_l}{\partial z} - A_h \varepsilon_l \rho_l g - \varepsilon_l S_{hw} \tau_l - F_{sf} \tag{3}$$

where P_l is the liquid phase pressure, Pa, τ_l is the shear stress between the liquid phase and the wall surface, N/m^2, F_{sf} is the interfacial force between liquid and solid phases, N, A_h is the area of the suspension layer, m^2, S_{hw} is the wetted perimeter, m, and g is the gravitational acceleration, taken as 9.8 m/s^2.

(d) Solid phase momentum equation:

$$\frac{\partial}{\partial t}(\varepsilon_s \rho_s v_s A_h) + \frac{\partial}{\partial z}(\varepsilon_s \rho_s v_s v_s A_h) = -\varepsilon_s A_h \frac{\partial P_l}{\partial z} - A_h \varepsilon_s \rho_s g - \varepsilon_s S_{hw} \tau_s + F_{sf} \tag{4}$$

where τ_s is the shear stress between the solid particles and the wall surface, N/m^2.

2.3 Performance Equation of Downhole Lifting Pump

The downhole lifting pump is an axial-flow pump, which operates by utilizing the high-speed rotation of its blades to generate axial thrust. As the impeller rotates, the liquid is propelled axially outward, creating a localized low-pressure region at the impeller inlet. This pressure differential continuously draws external fluid into the impeller. Axial guide vanes are employed to collect the fluid discharged from the impeller, remove its rotational component, and effectively convert part of its kinetic energy into pressure energy. This process reduces hydraulic losses within the impeller and ensures a relatively stable internal flow state.

Upon entering the axial-flow pump impeller, the liquid moves along a cylindrical flow surface, undergoing a compound motion that can be decomposed into three velocity components: absolute velocity $\vec{v}$, circumferential velocity $\vec{u}$, and relative velocity $\vec{w}$ [22]. The motion imparted by the

impeller's rotation is circular, while the motion of the liquid relative to the impeller is the relative velocity. The vector sum of the relative velocity and the circular motion constitutes the absolute velocity, which represents the motion of the liquid relative to a stationary reference frame. All three velocity vectors are tangent to the cylindrical flow surface and satisfy the relationship $\vec{v} = \vec{w} + \vec{u}$.

The three velocity vectors of any liquid particle can be formed into a velocity triangle, which can be used to summarize the motion law of the liquid inside the downhole lifting pump. The inlet and outlet of the impeller are particularly critical. For convenience, absolute velocity is usually decomposed into two mutually perpendicular components, denoted as v_u and v_m. Among them, the velocity component v_u along the circumferential direction is called the circumferential velocity, and its value is related to the head of the pump. The velocity v_m along the axial direction is called axial velocity, and its value is related to the flow rate of the pump. The triangle of import and export speed is shown in Fig. 2.

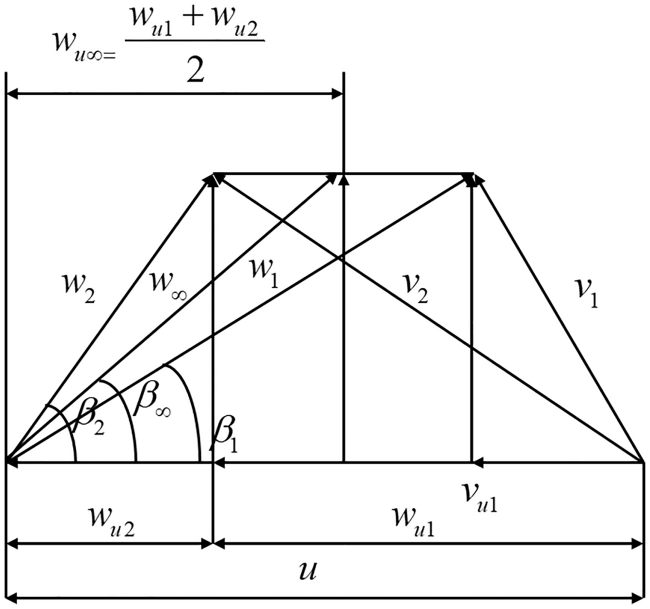

Figure 2: Triangle diagram of inlet and outlet of downhole lift pumps

Based on the inlet and outlet triangles of the downhole lifting pump, equations related to speed can be derived.

2.3.1 Speed Triangle

Import speed triangle

(a) Circular velocity at the inlet:

$$u_1 = \frac{D\pi n}{60} \tag{5}$$

where D is the impeller diameter, m, n is the impeller speed of the downhole lifting pump, r/min.

(b) Circumferential velocity at the inlet:

The inlet circumferential velocity depends on the suction conditions and is usually 0.

$$v_{u1} = 0 \tag{6}$$

(c) Axial velocity at the inlet:

$$v_{m1} = \frac{4Q_m}{\pi \left(D^2 - d_h^{\,2}\right)} \tag{7}$$

where Q_m is the mixed fluid flow rate, m^3/s, d_h is the diameter of the wheel hub, m.

Export speed triangle

(a) Circumferential velocity at the outlet:

The exit circumferential velocity is usually equal to the inlet circumferential velocity.

$$u_2 = u_1 = u \tag{8}$$

(b) Axial velocity at the outlet:

The axial velocity at the outlet is usually equal to the axial velocity at the inlet.

$$v_{m2} = v_{m1} = v_m \tag{9}$$

Geometric mean of relative velocity

Because the circumferential velocity u at the inlet and outlet of the axial-flow impeller cascade is equal, the inlet and outlet velocity triangles can be superimposed. The geometric mean of the relative velocities at the inlet and outlet is referred to as the relative velocity of the incoming flow at infinity, or simply the geometric mean relative velocity, denoted as w_∞. Based on the velocity triangle, it can be expressed as:

$$w_\infty = \sqrt{v_m^2 + \left(\frac{w_{u2} + w_{u1}}{2}\right)^2} = \sqrt{v_m^2 + \left(u - \frac{v_{u2} + v_{u1}}{2}\right)^2} \tag{10}$$

When $v_{u1} = 0$, w_∞ can be expressed as follows:

$$w_\infty = \sqrt{v_m^2 + \left(u - \frac{v_{u2}}{2}\right)^2} \tag{11}$$

The direction of geometric mean of relative velocity can be expressed as:

$$\tan \beta_\infty = \frac{v_m}{u - (v_{u2}/2)} \tag{12}$$

After presenting the velocity-related expressions, it is necessary to formulate the corresponding energy-related expressions for the downhole lifting pump. To this end, a brief description of the pump's operating principle and hydraulic design theory is provided, serving as the basis for deriving the energy-related formulation.

2.3.2 Head Equation of Downhole Lifting Pump

The downhole lifting pump utilizes a rotating impeller to impart torque to the fluid, thereby inducing axial motion. An axial-flow pump converts externally supplied mechanical energy into fluid energy. Based on the momentum equation, the theoretical head equation of an axial-flow pump can be derived to describe the relationship between the energy absorbed per unit weight of fluid from the impeller and the change in the fluid's angular momentum per unit time. This formulation also reflects the impeller's performance characteristics in the downhole lifting pump, specifically the conversion

of energy between theoretical head and fluid velocity. The theoretical head expression is given as follows [23]:

$$H_T = \frac{u\Delta v_u}{g} = \frac{u\left(v_{u2} - v_{u1}\right)}{g} \tag{13}$$

When $v_{u1} = 0$, H_T can be expressed as follows:

$$H_T = \frac{uv_{n2}}{g}H \tag{14}$$

2.3.3 Basic Equations for Designing Blades Using Lift Method

The lift method is the earliest and most enduring approach for designing the impeller blades of axial-flow pumps. This method draws on the aerodynamic principles governing aircraft wing motion to determine the blade profile, representing a semi-theoretical, semi-empirical design approach. The underlying assumptions of the lift method are as follows:

(1) The number of blades is small;

(2) The mutual interference between airfoils is minimal;

(3) The flow around an airfoil within a cascade is similar to that around an isolated airfoil.

Under these assumptions, a single-airfoil design can be applied, with mutual interference effects accounted for through appropriate corrections. The correction factors are typically obtained from experimental data.

By analyzing the energy transfer mechanism of the downhole lifting pump using the lift principle, the fundamental energy equation of the pump can be derived. This equation is expressed as follows:

$$C_y\left(l/t\right) = \frac{2\Delta v_u}{w_\infty}\frac{1}{1 + \tan\lambda/\tan\beta_\infty} \tag{15}$$

In this equation, the parameters can be classified into two categories: structural parameters of the downhole lifting pump and motion parameters of the fluid. Among them, C_y, l/t, and λ represent the structural parameters of the downhole lifting pump. Specifically, C_y is the lift coefficient of downhole lift pump, l/t is the density of underground lift pump blade grid, λ the tangent value of the angle between lift and resultant force can be expressed as the ratio of the drag coefficient of the downhole lift pump to the lift coefficient. The motion parameters of the liquid are Δv_u, ω_∞, and $\tan\left(\beta_\infty\right)$, and can be obtained from the triangle of inlet and outlet velocities, which have been listed in the previous text and will not be repeated here. This equation is actually an equation with unknown variables.

2.3.4 Hydraulic Efficiency of Downhole Lifting Pump

Fluid flow through the passage of a downhole lifting pump is accompanied by hydraulic friction losses, as well as additional hydraulic losses caused by impact, flow separation, and changes in velocity direction and magnitude, all of which result in energy dissipation. The energy lost per unit mass of fluid within the pump's flow passage is referred to as the hydraulic loss of the pump and is typically evaluated in terms of hydraulic efficiency.

For downhole lifting pumps, hydraulic efficiency is generally defined as the ratio of the pump's actual head to its theoretical head, accounting for hydraulic losses occurring within both the impeller and the guide vanes. Its value can be estimated using the method proposed by Guan [24], with the

corresponding estimation formula expressed as follows:

$$\eta_h = 1 + 0.083 \lg \sqrt[3]{\frac{Q_m}{n}} \tag{16}$$

2.3.5 Actual Head of Downhole Lifting Pump

Based on the previously defined hydraulic efficiency of the downhole lifting pump, the expression for its actual head can be written as:

$$H = H_T \eta_h \tag{17}$$

2.4 Auxiliary Equations

To close the above system of basic equations, corresponding auxiliary equations are introduced. These include geometric relationships, expressions for the physical properties of the solid–liquid phases, and formulations describing the forces acting on the solid–liquid phases.

2.4.1 Geometric Relationship Expression

(1) Hydraulic radius of annulus:

$$D_h = D_o - D_i \tag{18}$$

where D_o is the inner diameter of the wellbore, m; D_i is the outer diameter of the three channel drill pipe outer pipe, m.

(2) Suspended layer area:

For mixed-flow models applicable to vertical wells, the area of the suspended layer is equal to the annular cross-sectional area, which can be expressed as:

$$A_h = \frac{\pi}{4}\left(D^2{}_o - D^2{}_i\right) \tag{19}$$

(3) Wet perimeter:

The wetted perimeter is defined as the length of the boundary between the fluid and the solid wall surface at a given flow cross-section. For mixed-flow models applicable to straight wells, the wetted perimeter is equal to the circumference of the annulus and can be expressed as:

$$S_{hw} = \pi\left(D_o + D_i\right) \tag{20}$$

2.4.2 Expression of Physical Property Parameters

(1) Expressions for solid and liquid phase volume fractions:

For the Euler-Euler two fluid model, the sum of the volume fractions occupied by the two phases is equal to 1.

$$\varepsilon_l + \varepsilon_s = 1 \tag{21}$$

(2) Suspended layer density:

$$\rho_m = \varepsilon_l \rho_l + \varepsilon_s \rho_s \tag{22}$$

(3) Effective viscosity of fluids:

Most drilling fluids are non-Newtonian, among which the power-law model is the most widely used rheological model in engineering practice. Its main characteristics are:

(1) The constitutive equation is simple, containing only two constants that characterize rheological properties and have clear physical meanings;

(2) The equation can be readily linearized.

Therefore, in this study, the drilling fluid is modeled as a power-law fluid, and its effective viscosity is expressed as follows:

$$\mu_e = K\left(\frac{2n+1}{3n}\right)^n \frac{(D_h)^{1-n}}{(12u_l)^{1-n}} \tag{23}$$

where K is the viscosity coefficient of the drilling fluid, Pa·s^n, which is a characteristic ratio parameter used to characterize the viscosity of fluids, n is the flowability index of drilling fluid, dimensionless, used to characterize the degree to which the fluid deviates from Newtonian characteristics. When $n = 1$, it represents a Newtonian fluid. When $n > 1$, the fluid exhibits shear thickening characteristics, and at this time, the fluid is an expansive plastic fluid. When $n < 1$, the fluid exhibits shear dilution characteristics and is a pseudoplastic fluid.

(4) Liquid phase Reynolds number:

$$\mathrm{Re} = \frac{\rho_m |u_l| D_h}{\mu_e} \tag{24}$$

(5) Solid phase Reynolds number:

$$\mathrm{Re}_s = \frac{d_s \varepsilon_l \rho_l |u_l - v_s|}{\mu_e} \tag{25}$$

where d_s is the diameter of the solid particles, m.

2.4.3 Force Expression

(1) Shear stress between fluid and wall:

$$\tau_l = \frac{1}{2} f_l \rho_l |u_l| u_l \tag{26}$$

where f_l is the friction coefficient between the fluid and the wall, dimensionless.

$$f_l = \begin{cases} \dfrac{24}{\mathrm{Re}}, \mathrm{Re} \le 3470 - 1370n \\ \dfrac{0.046}{\mathrm{Re}^{0.2}}, \mathrm{Re} > 3470 - 1370n \end{cases} \tag{27}$$

(2) Shear stress between solid particles and wall:

$$\tau_s = \frac{1}{2} f_s \rho_s |v_s| v_s \tag{28}$$

where f_s is the friction coefficient between solid particles and the wall, dimensionless.

$$f_s = \frac{0.206}{v_s^{1.22}} \tag{29}$$

2.4.4 Interphase Forces between Solid-Liquid Phases

The exchange and transfer of momentum between the fluid and solid particles occur through various interphase forces, including drag, lift, buoyancy, virtual mass force, Brownian force, Saffman force, Bassett force, and others. Among these, drag is the most significant interphase force, exerting a pronounced influence on particle flow behavior. Therefore, in this study, other interphase forces are neglected, and only the interphase drag force is considered. The expression for the interphase drag force is given as follows [25]:

$$F_{sf} = J\,|u_l - v_s|\,(u_l - v_s) \tag{30}$$

The expression for J in the formula is as follows:

$$J = \frac{3\varepsilon_s A_h C_d \rho_l}{4 d_s \left(1-\varepsilon_s\right)^{1.65}} \tag{31}$$

where C_d is the drag coefficient, dimensionless.

$$\begin{cases} C_d = \frac{24}{\mathrm{Re}_s}\left(1 + 0.15\mathrm{Re}_s^{\,0.687}\right), \mathrm{Re}_s \le 500 \\ C_d = 0.44, \mathrm{Re}_s > 500 \end{cases} \tag{32}$$

3 Model Solving

3.1 Model Discretization

When applying the finite difference method to discretize the model in both the time and spatial domains, the temporal grid is generated based on a preset total simulation time and divided into uniform time steps. In the spatial domain, the hydraulic-lift dual-gradient drilling annulus flow model simplifies the solid–liquid two-phase flow to a one-dimensional flow along the wellbore axis, with emphasis on the axial distribution characteristics of annular pressure. Accordingly, a one-dimensional spatial grid is adopted, extending from the bottomhole to the wellhead along the fluid flow direction. The spatial mesh arrangement used for calculating wellbore annular pressure is illustrated in Fig. 3.

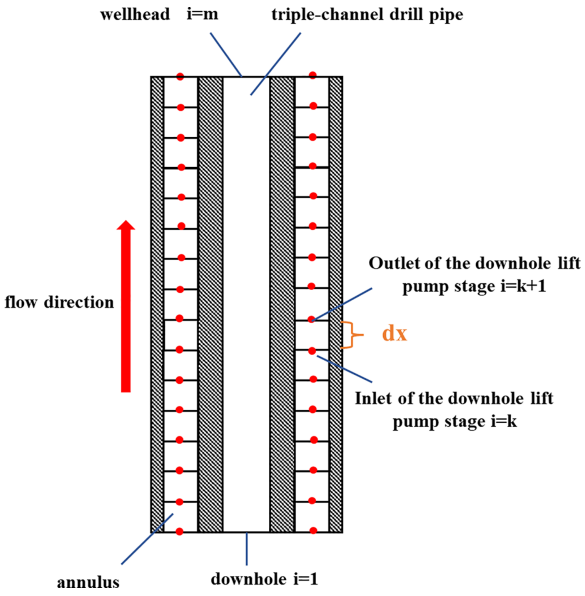

Figure 3: Schematic diagram of spatial grid division

3.2 Boundary Conditions

In the hydraulic-lift dual-gradient drilling annulus flow mathematical model, the boundary conditions are classified into two types: velocity boundaries and pressure boundaries. The velocity boundaries include the cuttings velocity at the bottomhole and the drilling fluid velocity at the bottomhole. The pressure boundaries comprise the wellhead pressure and the downhole lifting pump pressure.

The expression for the velocity of cuttings in the wellbore annulus (flow velocity of cuttings at the drill bit) is:

$$(v_s)_0 = \frac{D^2{}_0 ROP}{(D^2{}_0 - D^2{}_i)} \tag{33}$$

where ROP is the mechanical drilling speed, m/s. The expression for the flow rate of drilling fluid in the wellbore annulus is:

$$(u_l)_0 = \frac{4Q}{\pi \left(D_o^2 - D_i^2\right)} \tag{34}$$

where Q is the drilling fluid displacement, L/s. The expression for wellhead pressure is:

$$(P_l)_m = P_p \tag{35}$$

where P_p is the wellhead pressure, Pa.

The action of the downhole lifting pump can be used as a boundary condition for the hydraulic lifting dual-gradient drilling annulus flow mathematical model. Assuming that the downhole lifting pump corresponds to the spatial grid k node, the fluid at the $k+1$ node will obtain a certain amount of pressure energy from the k node lifting pump and be lifted to the surface. The expression for this boundary condition is:

$$(P_l)_{k+1} = (P_l)_k + \rho_m g H \tag{36}$$

3.3 Solution Method

Given the strong nonlinear coupling of the governing equations, which involve multiple interrelated unknowns, the SETS method is employed in this study to obtain the solution [26]. Originally developed for nuclear reactor safety analysis, the core concept of the SETS method is to divide the computation into two stages: a prediction step and a correction step. During the solution process, the SETS method applies a semi-implicit discretization scheme to the continuity and momentum equations, while explicitly treating the transport terms of density, energy, and momentum at element boundaries. This approach effectively enhances the numerical stability of the discretized equations and removes the restriction imposed by the Courant time step size. The solution procedure for the hydraulic-lift dual-gradient drilling annulus flow model is illustrated in Fig. 4.

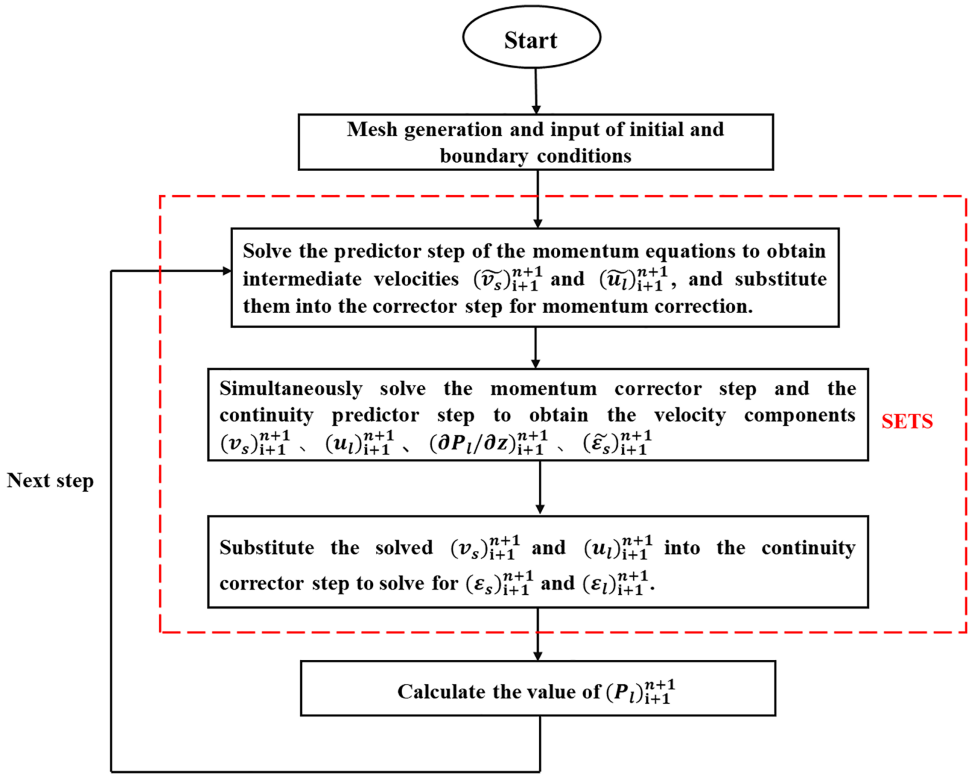

Figure 4: Theoretical model solution process

4 Model Validation

To verify the accuracy of the proposed model, experimental tests were carried out. Fig. 5 presents the schematic layout of the experimental system. The experimental setup employed wellbore dimensions consistent with those in the theoretical model: a simulated wellbore diameter of 0.252 m, a simulated drill string diameter of 0.168 m, a horizontal wellbore length of 11.015 m, and five lift pump sections. Based on the theoretical model, the annular pressure distribution was calculated at different axial positions in the wellbore annulus (h = 5.556, 6.356, 7.22, 10.1, 11.015 m) under various drilling fluid pump inflow rates. The calculated results were then compared with the corresponding experimental measurements.

Fig. 6 presents the pressure distribution at various measurement points in the wellbore annulus under different drilling fluid pump flow rates (corresponding to different backpressure valve openings in the experiment) for both conventional drilling and hydraulic-lift dual-gradient drilling. In both cases, the annular pressure distribution predicted by the model closely matches the experimental measurements, demonstrating a high degree of consistency in distribution trends. This agreement verifies the effectiveness and accuracy of the proposed model.

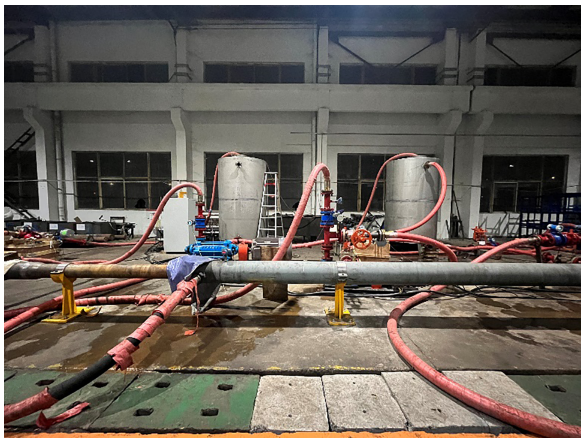

Figure 5: Layout of hydraulic lift type dual-gradient drilling indoor physical simulation experiment system

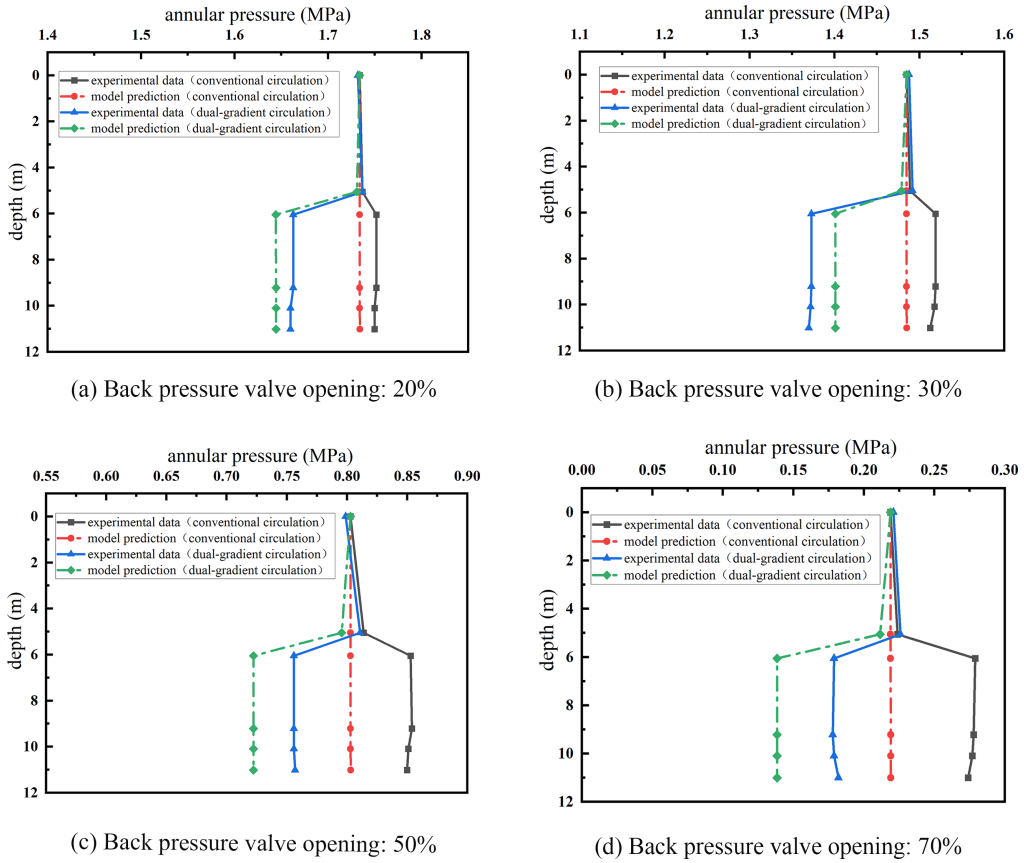

(a) Back pressure valve opening: 20%

(b) Back pressure valve opening: 30%

(c) Back pressure valve opening: 50%

(d) Back pressure valve opening: 70%

Figure 6: Comparison of model predicted data with experimental data for different pressure return valve openings

The annular pressures calculated by the model at various measurement points were compared with the corresponding experimental data, and the maximum and average errors were determined for

both conventional drilling and hydraulic-lift dual-gradient drilling. The results of the error analysis are summarized in Table 1, while the comparison between experimental measurements and model predictions is illustrated in Fig. 7. For conventional drilling, the maximum average error across different drilling fluid pump inflow rates was 14.3%, and the average error gradually decreased as the opening of the drilling fluid return pipeline was reduced. Under hydraulic-lift dual-gradient drilling conditions, the maximum average error was 16.4%, with a similar trend of decreasing average error as the return pipeline opening decreased. These results indicate that the annular pressures predicted by the model deviate only slightly from the experimental measurements, thereby confirming the model's effectiveness.

Table 1: Error analysis of model calculation results and experimental results

Back pressure valve opening (%)	Mud pumping flow rate (L/s)	Max error under normal conditions (%)	Avg error under normal conditions (%)	Max error under dual-gradient conditions (%)	Avg error under dual-gradient conditions (%)
25	7.61	1.02	0.67	1.12	0.76
35	10.61	2.23	1.46	2.28	1.60
50	13.72	5.96	4.05	4.57	3.38
70	13.89	21.5	14.3	23.9	16.4

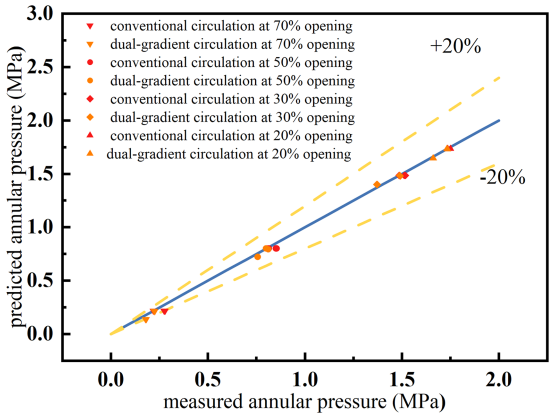

Figure 7: Plot of experimental measurements vs. model prediction error analysis

As shown in Table 1 and Fig. 7, the model's predictions match the experimental results closely for backpressure valve openings of 25%, 35%, and 50%, with maximum errors below 5%. However, at a 70% backpressure valve opening, the maximum error increases to 23.9%. This is primarily due to the nonlinear behavior of the backpressure valve at high openings, which leads to greater fluctuations in fluid pressure and flow. In future work, we plan to address this issue by replacing the backpressure valve with an infinitely adjustable electric-driven pump, enabling more precise flow control and reducing such discrepancies.

5 Case Analysis

To investigate the annular flow characteristics of hydraulic-lift dual-gradient drilling, calculations and analyses were performed using a simulated well. A land-based vertical well with a depth of 8000 m, equipped with a downhole lifting pump of optimized parameter configuration, was selected as the reference case. The drilling parameters and downhole lifting pump specifications are summarized in Table 2.

Table 2: Basic data of the algorithm

Drilling parameters	Value	Downhole lift pump parameters	Value
Vertical depth/m	8000	Rotational speed/r/min	1250
Borehole diameter/m	0.2159	Impeller diameter/m	0.2
Drill string diameter/m	0.127	Hub diameter/m	0.13
Drilling fluid density/kg/m^3	1100	Number of blades	5
Drilling fluid flow rate/L/s	40	Blade pitch/mm	188.5
Flow behavior index	0.68	Blade solidity	0.94
Consistency index	0.2	Number of impeller (Guide Vane) stages	5
Cuttings density/kg/m^3	2650	Lift coefficient	0.53
Cuttings diameter/m	0.005	Drag coefficient	0.009
Rate of penetration/m/h	30	Number of pump stages	10

5.1 Drilling Fluid Flow Rate

As shown in Fig. 8, the solid-phase volume fraction in the annulus decreases progressively with increasing drilling fluid flow rate. This occurs because a higher drilling fluid flow rate directly increases the liquid-phase velocity, thereby enhancing the drag force exerted on the cuttings. The increased drag accelerates the solid-phase flow, facilitating the suspension and transport of cuttings particles, which effectively reduces the solid-phase volume fraction. Moreover, the figure indicates that the variation in solid-phase volume fraction is more pronounced within the low-flow-rate range (25–35 L/s).

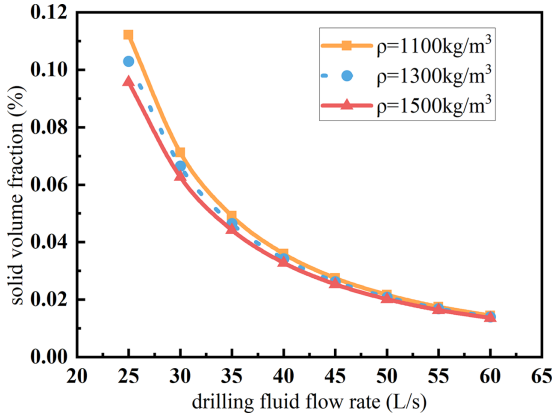

Figure 8: Variation of solid phase volume fraction with drilling fluid flow rate after stabilization

As shown in Fig. 9, the reduction in bottomhole pressure diminishes as the drilling fluid flow rate increases. This behavior arises because, within a certain flow range, an increase in the discharge flow rate of the downhole lifting pump leads to a decrease in pump head. Consequently, increasing the drilling fluid displacement reduces the pump head, which in turn lessens the reduction in bottomhole pressure. This trend also partially reflects the operating characteristics of the downhole lifting pump.

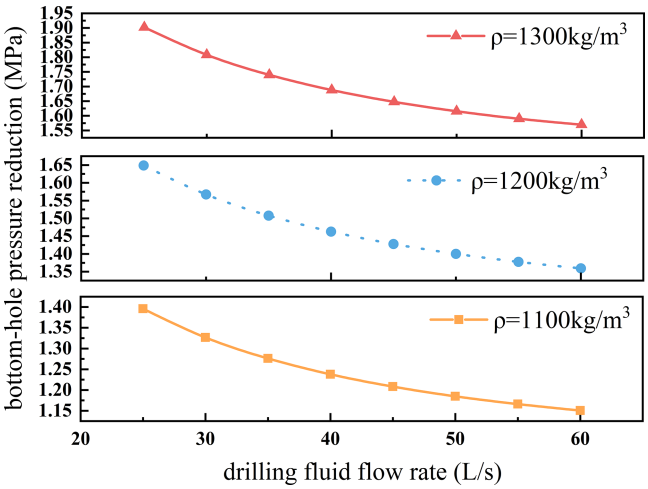

Figure 9: Changes in bottomhole pressure reduction with drilling fluid flow rate

5.2 Drilling Fluid Viscosity

As shown in Fig. 10, the solid-phase volume fraction in the annulus decreases with increasing drilling fluid viscosity, with the maximum cuttings concentration reduced by up to 40%. This occurs because higher drilling fluid viscosity increases the drag force exerted on the cuttings, thereby enhancing cuttings lifting efficiency. This effect is more pronounced at low drilling fluid flow rates, where the volume fraction of settled cuttings decreases accordingly. As shown in Fig. 11, the reduction in bottomhole pressure diminishes as drilling fluid viscosity increases.

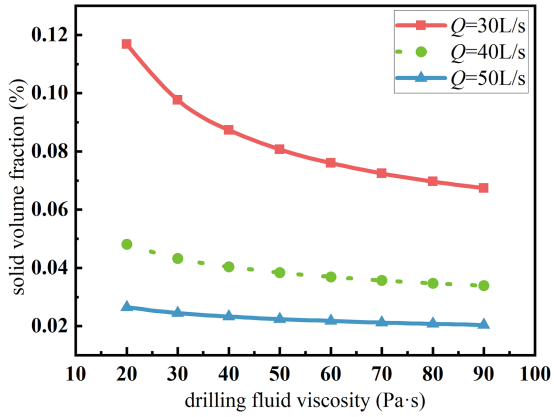

Figure 10: Variation of solid phase volume fraction with drilling fluid viscosity after stabilization

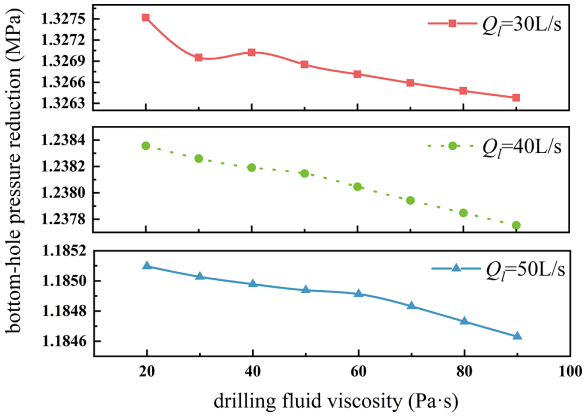

Figure 11: Changes in bottomhole pressure reduction with drilling fluid viscosity

5.3 Downhole Lifting Pump Speed

As shown in Fig. 12, the reduction in bottomhole pressure increases with increasing impeller speed of the downhole lifting pump. When the pump speed rises from 650 to 1450 r/min, the reduction in bottomhole pressure increases by 2.06 MPa. This is because a higher impeller speed corresponds to greater input power to the pump section, enabling the downhole lifting pump to generate a higher head. The increased pressure energy imparted to the fluid as it passes through the pump results in a lower bottomhole pressure and, consequently, a greater reduction in bottomhole pressure.

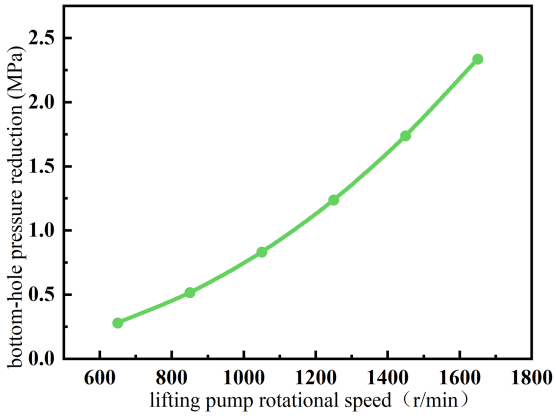

Figure 12: Wellbore pressure reduction with the change of lifting pump section

5.4 Number of Sections of Downhole Lifting Pump

As shown in Fig. 13, the reduction in bottomhole pressure increases linearly with the number of lift pump sections. When the number of pump sections increases from 10 to 35, the reduction in bottomhole pressure rises by 3.03 MPa. This occurs because adding pump sections is equivalent to connecting multiple downhole lifting pumps in series, which produces a linear increase in head and, consequently, a linear increase in pressure energy. As a result, the pressure in the section from the lift pump to the bottomhole decreases, leading to a proportional increase in the reduction of bottomhole pressure.

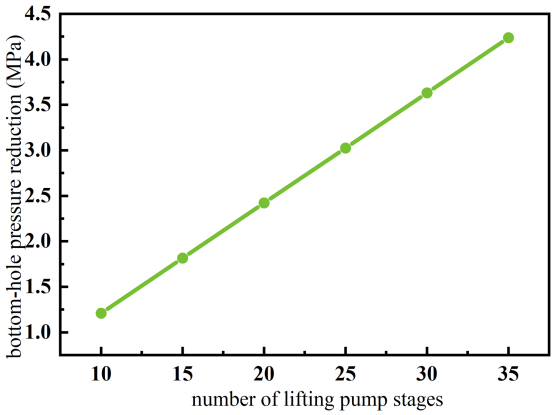

Figure 13: Wellbore pressure reduction with the change of lifting pump section

6 Conclusions

(1) This study presents an innovative theoretical model for hydraulic-lift dual-gradient drilling annulus flow, specifically tailored for ultra-deep vertical wells. The model integrates solid–liquid two-phase mixed flow characteristics and the dynamic effects of downhole lifting pumps. By solving the nonlinear, strongly coupled system of equations using the SETS method, we significantly enhance the computational efficiency and stability of the model.

(2) A comprehensive comparison with experimental data was conducted using wellbore dimensions and lift pump parameters consistent with the experimental setup. The results demonstrate that the model's predictions are highly accurate, with a maximum average error of only 16.4%. This confirms the model's reliability and applicability for predicting annular pressure in hydraulic-lift dual-gradient drilling operations.

(3) Numerical analysis of key operational parameters—including drilling fluid flow rate, viscosity, lift pump speed, and the number of pump sections—reveals the following insights: Increasing both the flow rate and viscosity of the drilling fluid effectively reduces cuttings concentration in the annulus and enhances cuttings suspension. Additionally, raising the speed and number of pump sections significantly improves pressure energy transmission and increases the range of bottomhole pressure control. These findings underscore the critical role of these parameters in regulating the annular pressure field and bottomhole pressure, providing a solid theoretical foundation for the optimization and design of hydraulic-lift dual-gradient drilling systems.

(4) In future work, we plan to develop an optimized hydraulic-lift pump parameters model to improve pressure control accuracy within the existing model. Additionally, integrating real-time monitoring systems and considering variable fluid properties under different conditions will further enhance the model's performance and applicability for complex drilling scenarios.

Acknowledgement: Not applicable.

Funding Statement: The project is supported by The Key Core Technology Research Project of China National Petroleum Corporation (2024ZG26), the Youth Science and Technology Program of China National Petroleum Corporation (2024DQ03086), the Joint Foundation Program of National Natural Science Foundation of China (U24B2030), National Science and Technology Major Project (2025ZD1401905).

Author Contributions: The authors confirm contribution to the paper as follows: Conceptualization, Yufei Chen, Jinping Yuan, and Mu Li; methodology, Yufei Chen; software, Yufei Chen; validation, Yufei Chen, Jinping Yuan, Kerou Liu, Jingyu Zhu, Mu Li, and Hao Wang; formal analysis, Yufei Chen and Kerou Liu; investigation, Yufei Chen and Jingyu Zhu; resources, Yufei Chen, Jinping Yuan, and Mu Li; data curation, Yufei Chen, Jingyu Zhu, and Hao Wang; writing—original draft preparation, Yufei Chen; writing—review and editing, Yufei Chen, Jinping Yuan, Kerou Liu, Mu Li, and Yafei Li; visualization, Yufei Chen and Mu Li; supervision, Jinping Yuan and Mu Li; project administration, Jinping Yuan and Mu Li; funding acquisition, Jinping Yuan. All authors reviewed the results and approved the final version of the manuscript.

Availability of Data and Materials: Not applicable.

Ethics Approval: Not applicable.

Conflicts of Interest: The authors declare no conflicts of interest to report regarding the present study.

References

1. Yu YJ, Xia XJ, Wang ZG. Progress and application of the key technologies of deep and ultra-deep well ce-menting. Xinjiang Oil Gas. 2023;19(2):24–33. (In Chinese).
2. Wang HG, Han HC, Ji GD, Chen CC, Lv ZH, Chen WF, et al. Progress and challenges of drilling and completion technologies for deep, ultra-deep and horizontal wells of CNPC. China Pet Explor. 2023;28(3):1. (In Chinese). doi:10.2523/iptc-24918-ms.
3. Zhang RY. Study on prediction and control method of wellbore pressure in deepwater multi-gradient drilling [dissertation]. Beijing, China: China University of Petroleum (Beijing); 2022. (In Chinese).
4. Smith KL, Gault AD, Witt DE, Weddle CE. SubSea MudLift drilling joint industry project: delivering dual-gradient drilling technology to industry. In: SPE Annual Technical Conference and Exhibition; New Orleans, LA, USA; 2002. SPE-71357-MS.
5. Smith D, Winters W, Tarr B, Ziegler R, Riza I, Faisal M. Deepwater riserless mud return system for dual gradient tophole drilling. In: SPE/IADC Managed Pressure Drilling and Underbalanced Operations Conference and Exhibition; Kuala Lumpur, Malaysia; 2010. SPE-130308-MS.
6. Matthew Daniel Martin. Managed pressure drilling techniques and tools [~~Doctoral~~ dissertation]. College Station, TX, USA: Texas A&M University, 2006.
7. Wang G, Li X, Zhong L, Lv Z. Research on the stability of the spacer fluid interface in dual-layer pipe dual-gradient drilling. Processes. 2023;11(8):2395. doi:10.3390/pr11082395.
8. Chen Q, Deng Q, Tan L, Qi G, Zhang J. Status and prospects of dual-gradient drilling technologies in deep-water wells. Front Energy Res. 2022;10:920178. doi:10.3389/fenrg.2022.920178.
9. Wang G, Lv Z, Zhong L, Li Z, Fu Q, Li Y, et al. Hydraulic modeling study and control algorithm design of double-layer pipe dual-gradient drilling. Geoenergy Sci Eng. 2024;240:212926. doi:10.1016/j.geoen.2024.212926.
10. Wang G, Lv Z, Zhong L, Li Z, Fu Q, Li Y, et al. Double-layer pipe dual-gradient drilling well-bore pressure calculation model and parameters optimization. Geoenergy Sci Eng. 2023;230(2):212249. doi:10.1016/j.geoen.2023.212249.
11. Gavignet AA, Sobey LJ. Model aids cuttings transport prediction. J Petroleum Technol. 1989;41(9):916–21. doi:10.2118/15417-pa.
12. Martins AL, Santana ML, Goncalves CJC, et al. Evaluating the transport of solids generated by shale instabilities in ERW drilling-part two: case studies. In: SPE International Conference on Horizontal Well Technology; Calgary, ~~Alberta~~, Canada; 1998. SPE-50380-MS.

13. Doron P, Granica DG, Barnea D. Slurry flow in horizontal pipes-experimental and modeling. Int J Multiphase Flow. 1987;13(4):535–47. doi:10.1016/0301-9322(87)90020-6.
14. Santana M, Martins AL, Sales JA. Advances in the modeling of the stratified flow of drilled cuttings in high angle and horizontal wells. In: The International Petroleum Conference and Exhibition of Mexico; Villahermosa, Mexico; 1998. SPE-39890-MS.
15. Naganawa S, Nomura T. Simulating transient behavior of cuttings transport over whole trajectory of extended reach wel. In: IADC/SPE Asia Pacific Drilling Technology Conference and Exhibition; Bangkok, Thailand; 2006. SPE-103923-MS.
16. Sun XF, Yao D, Sun SH, Ji GD, Yu FR, Sun MH, et al. A new transient calculation method of cuttings bed thickness based on drift flow model. Nat Gas Ind. 2022;42:85–92. (In Chinese).
17. Turkyilmazoglu M, Alotaibi A. Coating with Newtonian fluid by a two-parameter blade family leading to exact dynamic and thermal solutions. Chin J Phys. 2025;96:1191–202. doi:10.1016/j.cjph.2025.06.007.
18. Turkyilmazoglu M, Alotaibi A. Non-Newtonian fluid flows over deformable rotating disk: exact flow/heat solutions. Int Commun Heat Mass Transf. 2025;167:109211. doi:10.1016/j.icheatmasstransfer.2025.109211.
19. Guo XL, Wang ZM, Long ZH. Study on three-layer unsteady model of cuttings transport for extend-ed-reach well. J Pet Sci Eng. 2010;73(1–2):171–80.
20. Zhu N, Huang W, Gao D. Dynamic wavy distribution of cuttings bed in extended reach drilling. J Pet Sci Eng. 2021;198(3):108171. doi:10.1016/j.petrol.2020.108171.
21. Chen YF, Zhang H, Li J, Zhou Y, Lu Z, Ouyang Y, et al. Simulation study on cuttings transport of the wavy wellbore trajectory in the long horizontal wellbore. J Pet Sci Eng. 2022;215(8):110584. doi:10.1016/j.petrol.2022.110584.
22. Zhang KW. Principles of fluid machinery ~~(Volume 1),~~ Beijing, China: China Machine Press; 2000. (In Chinese).
23. Caridad J, Asuaje M, Kenyery F, Tremante A, Aguillón O. Characterization of a centrifugal pump impeller under two-phase flow conditions. J Pet Sci Eng. 2008;63(1):18–22. doi:10.1016/j.petrol.2008.06.005.
24. Guan XF. Modern pump theory and design. Beijing, China: China Astronautic Publishing House; 2011. (In Chinese).
25. Bizhani M, Kuru E. Critical review of mechanistic and empirical (semimechanistic) models for particle removal from sandbed deposits in horizontal annuli with water. SPE J. 2018;23(2):237–55. doi:10.2118/187948-pa.
26. Mahaffy JH. A stability-enhancing two-step method. J Comput Phys. 1982;46(3):329.